Impact of vegetation removal and soil aridation on diurnal temperature range in a semiarid region: Application to the Sahel

Liming Zhou*†, Robert E. Dickinson*, Yuhong Tian*, Russell S. Vose‡, and Yongjiu Dai§

*School of Earth and Atmospheric Sciences, Georgia Institute of Technology, Atlanta, GA 30332; ‡Climate Analysis Branch, National Climatic Data Center, Asheville, NC 28801; and §School of Geography, Beijing Normal University, Beijing 100875, China

Edited by Inez Y. Fung, University of California, Berkeley, CA, and approved September 25, 2007 (received for review January 11, 2007)

Increased clouds and precipitation normally decrease the diurnal temperature range (DTR) and thus have commonly been offered as explanation for the trend of reduced DTR observed for many land areas over the last several decades. Observations show, however, that the DTR was reduced most in dry regions and especially in the West African Sahel during a period of unprecedented drought. Furthermore, the negative trend of DTR in the Sahel appears to have stopped and may have reversed after the rainfall began to recover. This study develops a hypothesis with climate model sensitivity studies showing that either a reduction in vegetation cover or a reduction in soil emissivity would reduce the DTR by increasing nighttime temperature through increased soil heating and reduced outgoing longwave radiation. Consistent with empirical analyses of observational data, our results suggest that vegetation removal and soil aridation would act to reduce the DTR during periods of drought and human mismanagement over semiarid regions such as the Sahel and to increase the DTR with more rainfall and better human management. Other mechanisms with similar effects on surface energy balance, such as increased nighttime downward longwave radiation due to increased greenhouse gases, aerosols, and clouds, would also be expected to have a larger impact on DTR over drier regions.

drought | surface emissivity | longwave radiation | sensitivity test | surface energy balance

The global mean land surface air temperature has been steadily rising since the 1950s, primarily attributed to increased greenhouse gases, and this rising results largely from nighttime warming over some land areas as minimum temperature (T_{min}) increased much faster than maximum temperature (T_{max}) (1). Associated with such asymmetric warming is the reduction of the diurnal temperature range (DTR) (DTR = $T_{max} - T_{min}$) (1). The decrease in DTR has been observed over most locations over land since 1950 (2), but in many parts of the world this decline abated in the early 1980s (3), perhaps coincident with the reversal of global dimming (4). The DTR appears to continue to decrease in some rapidly industrializing locations such as southern China (5).

Changes in DTR can result from a number of mechanisms, all connected to the surface energy balance. The most obvious and widely recognized mechanism from a meteorological viewpoint is the reduction of DTR as a consequence of the increase of clouds, precipitation, and soil moisture (6, 7). Clouds, especially low clouds, decrease the daytime surface solar heating and increase nighttime downward longwave radiation. Evapotranspiration associated with soil moisture and precipitation can balance solar heating and further reduce T_{max}. These day-to-day changes in DTR aggregate to seasonal to multidecadal statistical connections between DTR and clouds/precipitation/soil moisture (7).

Other mechanisms such as changes in atmospheric circulation, greenhouse gases, aerosols, and land cover/use may also contribute to a decrease of the DTR (6, 8, 9). Increasing greenhouse gases can decrease DTR alone, but they have a larger impact when combined with the effects of water vapor, clouds, and soil moisture (10–13). Aerosols may have a small effect on DTR by reflecting solar radiation but can have larger effects through their modification of cloud properties and hence reduction of surface heating. Their nighttime effect of increased cloud cover, hence surface warming, may further increase T_{min} and hence reduce DTR (14).

Observational Data Analysis

Here we use a 5° by 5° global monthly T_{max}, T_{min}, and DTR dataset for the period 1950–2004 (3), along with global monthly precipitation (15), total cloud cover (16), and satellite-measured vegetation greenness (17) datasets, to generate annual and seasonal mean time series anomalies and estimate linear time trends by using ordinary least-squares (details are in *Data and Methods*). Consistent with previous studies (2, 3), the annual mean DTR is observed to have declined over most land areas [supporting information (SI) Fig. 6]. The largest decreases in the DTR are observed mostly over arid or semiarid regions such as the West African Sahel, parts of the Middle East and Mongolia, and North China where drought has occurred. We aggregated the observed DTR trends into a number of climate regions globally from dry to wet in terms of climatological annual mean precipitation and then analyzed the spatial dependence of the DTR trends on the annual precipitation by climate region. Interestingly, the negative linear fit between the DTR trends and the amount of precipitation is statistically significant at the 1% level, i.e., the drier the climate, the larger the reduction of the DTR (Fig. 1). We speculate that such a relationship may possibly reflect the effects of increased global greenhouse gases and/or aerosols on DTR over different ecosystems. Its further attribution, however, is beyond the scope of this study.

The West African Sahel was examined to investigate what other mechanisms aside from changes of clouds/precipitation can decrease DTR, because its reduction in the observed DTR is much larger than was expected (Fig. 1). The Sahel is one of the most climatically sensitive zones in the world (18) and has experienced a prolonged drought from the 1950s to the 1980s (19). Fig. 2 shows the spatial pattern of observed temperature trends and area-weighted average year-to-year variations of

Author contributions: L.Z. designed research; L.Z. and Y.T. performed research; L.Z. contributed new reagents/analytic tools; L.Z., R.E.D., Y.T., R.S.V., and Y.D. analyzed data; and L.Z., R.E.D., and Y.T. wrote the paper.

The authors declare no conflict of interest.

This article is a PNAS Direct Submission.

Abbreviations: CTL, control; DTR, diurnal temperature range; HV, half vegetation; HVLE, half vegetation and lower emissivity; NDVI, normalized difference vegetation index; NV, no vegetation; NVLE, no vegetation and lower emissivity.

†To whom correspondence should be addressed at: School of Earth and Atmospheric Sciences, Georgia Institute of Technology, 311 Ferst Drive, Atlanta, GA 30332. E-mail: lmzhou@eas.gatech.edu.

This article contains supporting information online at www.pnas.org/cgi/content/full/0700290104/DC1.

© 2007 by The National Academy of Sciences of the USA

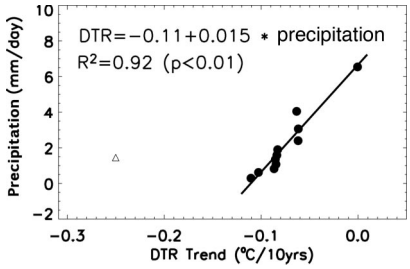

Fig. 1. Dependence of observed annual mean DTR trends (°C/10 yr) on climatological annual mean precipitation averaged by climate region for the period of 1950–2004. The 528 grid boxes were equally classified into 11 climate regions globally, from dry to wet, based on their climatological annual mean precipitation amount, and area-weighted regional average DTR trends and precipitation were calculated for those climate regions. A linear regression line was fitted by using least squares between the precipitation and the DTR trends. A two-tailed Student's *t* test was used to test whether the slope of the fitted line differs significantly from zero. The value masked with △ is from the Sahel.

T_{max}, T_{min}, DTR, cloud cover, and rainfall anomalies over the Sahel. There is a strong and statistically significant warming trend in T_{min} but a small and insignificant trend in T_{max}. As a result, the DTR has declined over almost all of the grid boxes over the Sahel. The strong downward trend of rainfall from the 1950s to the 1980s began to reverse slightly in 1983, as did the rainfall, cloud cover, vegetation greenness, and DTR, but with lags of several years (Fig. 2). Statistical analyses of time series show that interannual changes in DTR are significantly correlated inversely with those in rainfall and clouds (Table 1), especially in the wet season, as expected from reduced solar heating and increased soil moisture (7). However, the long-term DTR trend shows an opposite effect and so cannot be accounted for by a decrease in cloud cover, rainfall, and soil moisture due to drought. The trend of decreasing DTR (Fig. 1) cannot be a result of reduced daytime solar heating and wetter soils, therefore, it must involve net nighttime radiative heating, possibly from increases of greenhouse gases and/or of aerosols and their changes in clouds (20).

This current study explores mechanisms involving soil–vegetation impacts that may have contributed to some of the observed large changes of the DTR in the Sahel and other semiarid regions. Drought and human mismanagement (e.g., overgrazing, overfarming, and deforestation) over the Sahel have reduced soil wetness and vegetative cover/productivity, and thus have resulted in land degradation and soil erosion such as the reduction of soil fertility, particularly base cation content, organic matter content, pore space, and water-retention capacity (21). Such changes would modify the land surface albedo and emissivity and hence the surface radiation and energy budget. The emissivity decreases with decreasing leaf area and soil wetness (22, 23), whereas the albedo increases (24). Soils with less water and organic matter content have lower emissivities. Dry and dead vegetation has a lower emissivity than green vegetation because of its structure and content of water. Consequently, reduced vegetation cover and soil wetness and associated land degradation and soil erosion may have increased

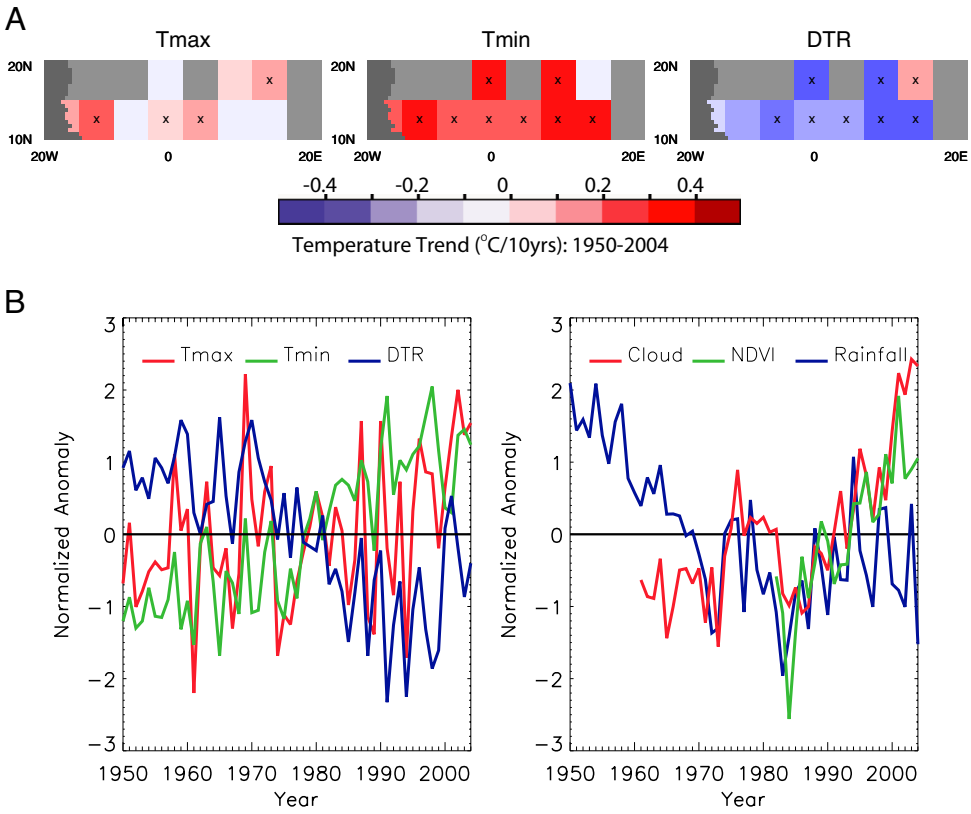

Fig. 2. Observed changes in temperatures, cloud cover, greenness, and rainfall over the Sahel. (*Upper*) Spatial patterns of observed trends (°C/10 yr) in annual mean T_{max}, T_{min}, and DTR over the 5° by 5° grid boxes in the Sahel for the period of 1950–2004. The trends marked with ''x'' within the grid boxes are statistically significant at the 5% level. A two-tailed Student's *t* test was used to test whether the DTR trend differs significantly from zero. (*Lower*) Area-weighted average observed annual mean anomalies of T_{max}, T_{min}, DTR, rainfall, cloud cover, and satellite-measured normalized difference vegetation index (NDVI) over the Sahel for the period of 1950–2004. All of the variables (*Lower*) were normalized for visualization purpose only by subtracting their means divided by their standard deviation. The cloud data are available only from 1961 to 2004, and the NDVI data are available only from 1982 to 2004.

Table 1. Statistical relationships between changes in temperature and changes in rainfall, clouds, and NDVI over the Sahel

			$Y = \beta_0 + \beta_1 X + \beta_2$ time $+ \varepsilon$			$\Delta Y = \beta_0 + \beta_1 \Delta X + \varepsilon$	
Season	Y	X	R^2	β_1	β_2, °C/10 yr	R^2	β_1
				1950–2004			
JAS	T_{max}	P	0.80	**−0.79**	0.015	0.78	**−1.00**
	T_{min}		0.69	**−0.22**	**0.226**	0.31	**−0.31**
	DTR		0.59	**−0.56**	**−0.208**	0.68	**−0.68**
Annual	T_{max}		0.17	−0.35	0.045	0.15	**−0.84**
	T_{min}		0.73	0.22	**0.344**	0.03	0.33
	DTR		0.61	**−0.62**	**−0.303**	0.42	**−1.23**
				1961–2004			
JAS	T_{max}	C	0.38	**−0.10**	**0.326**	0.33	**−0.17**
	T_{min}		0.69	**−0.07**	**0.387**	0.23	**−0.07**
	DTR		0.08	−0.03	−0.065	0.21	**−0.10**
Annual	T_{max}		0.16	0.00	0.110	0.10	**−0.07**
	T_{min}		0.69	**−0.04**	**0.450**	0.01	−0.02
	DTR		0.46	**0.04**	**−0.338**	0.06	−0.05
				1982–2004			
Annual	T_{max}	VI	0.29	−10.21	**0.433**	0.06	−17.02
	T_{min}		0.36	**−25.48**	**0.528**	0.24	**−24.97**
	DTR		0.06	14.43	−0.109	0.01	5.82

JAS, July–August–September; P, precipitation (mm/day); C, cloud (%); VI, normalized difference vegetation index (NDVI); T_{max}, maximum temperature (°C); T_{min}, minimum temperature (°C); DTR, diurnal temperature range (°C). Regression coefficients, β_0 (not shown), β_1, and linear time trends, β_2, in boldface are statistically significant at the 5% level. A two-tailed Student's t test was used to test whether β_1 or β_2 differs significantly from zero. To avoid spurious regressions (43), two regression models, detrending and differentiating the original time series, were used to estimate relationships between changes in temperature and changes in rainfall, clouds, and NDVI (Fig. 2). The results between NDVI and temperatures are not shown for the wet season (JAS) because the effects of clouds and rainfall dominate the temperature changes and thus mask the contribution from vegetation.

albedo and decreased emissivity over the Sahel. Higher albedo reduces the absorption of solar radiation, but such an effect is largely cancelled by the increase of incoming radiation due to less cloud cover (25–28). Lower emissivity reduces outgoing longwave radiation and thus raises temperatures (29), especially over arid and semiarid regions during nighttime when the combined effects of longwave radiation, surface roughness, wind speed, soil heat capacity, and soil heat conduction influence energy exchange.

Climate Model Simulations

To quantify the vegetation–soil impacts on the Sahelian DTR changes, we have used the latest Community Land Model (CLM3.1) coupled with the Community Atmosphere Model (CAM3.1) (30, 31). CLM3.1 continues to be improved and has been used as the land component of the Community Climate System Model for extensive coupled climate model simulations contributed to the Intergovernmental Panel on Climate Change (IPCC). To ensure an accurate description of vegetation type, fractional cover, and amount, a new land surface dataset created from multiple high-quality Moderate-resolution Imaging Spectroradiometer (MODIS) products (32) was added to the CLM3.1 for this study. The new dataset relative to the default has a more realistic seasonal cycle of leaf area index (LAI) from dry to wet season over tropical regions and improves the simulation of the land surface climate and energy balance in the model. Vegetation–soil impacts were imposed through modification of soil emissivity and vegetation cover. Impacts of modification of surface albedo have been examined in many contexts (28, 33–35) and thus will not be discussed here.

We performed five model simulations, one control run, and four experiments, referred to as control (CTL), no vegetation and lower emissivity (NVLE), no vegetation (NV), half vegetation and lower emissivity (HVLE), and half vegetation (HV), over the Sahel. For CTL, the Sahelian soil and vegetation were unchanged. For NVLE and NV, all vegetation was replaced by bare soil, which is equivalent to moving the Sahara Desert southward. For HVLE and HV, half of the vegetation cover was removed, which represents a less dramatic modification. The soil emissivity of 0.96 as used in CTL was unchanged in NV and HV, but it was replaced by 0.89 in NVLE and HVLE. The soil emissivity of 0.89 is a typical satellite-derived value averaged over the Sahelian barren pixels from the MODIS/Advanced Spaceborne Thermal Emission and Reflection Radiometer (ASTER) (29, 36). Here we assumed a soil emissivity of 0.96 (0.89) as the value before (after) the extreme effects of vegetation removal and soil aridation. The global land surface emissivity observed in MODIS data for barren and sparsely vegetated areas ranges from 0.87 to 0.97 (37). Such large variations can be mainly attributed to differences in underlying soil conditions and the amount of vegetation. For a large area like the Sahel, a change of soil emissivity from 0.96 to 0.89 might be expected to occur over a much longer time scale. However, such a change may have occurred over half a century as a consequence of drought, human-induced reduction in vegetation amount and soil organic content, and land degradation. Although a removal of all vegetation and a reduction of soil emissivity by 0.07 may be extreme assumptions, they allow us to isolate the sensitivity of the DTR to these factors, as commonly done in climate sensitivity studies. The difference between NVLE and NV or HVLE and HV separates the impacts of changes in soil emissivity from those in vegetation on surface air temperature. All five simulations were carried out for 20 years by using Community Land Model 3.1/Community Atmosphere Model 3.1 with resolution at about 2.8° × 2.8°. Climatological sea surface temperature and sea ice were used, and other soil properties were kept the same in all simulations. The first 2 years of model runs were used as spinup and the last 18-year results were analyzed in this study. The model outputs are 3-hr averages from each time step (20 min). For each day, the T_{max} and T_{min} were chosen from eight of the simulated 2-m-high surface air temperatures. Because this study is focused on the vegetation–soil feedbacks on DTR, most of our results are shown for clear-sky

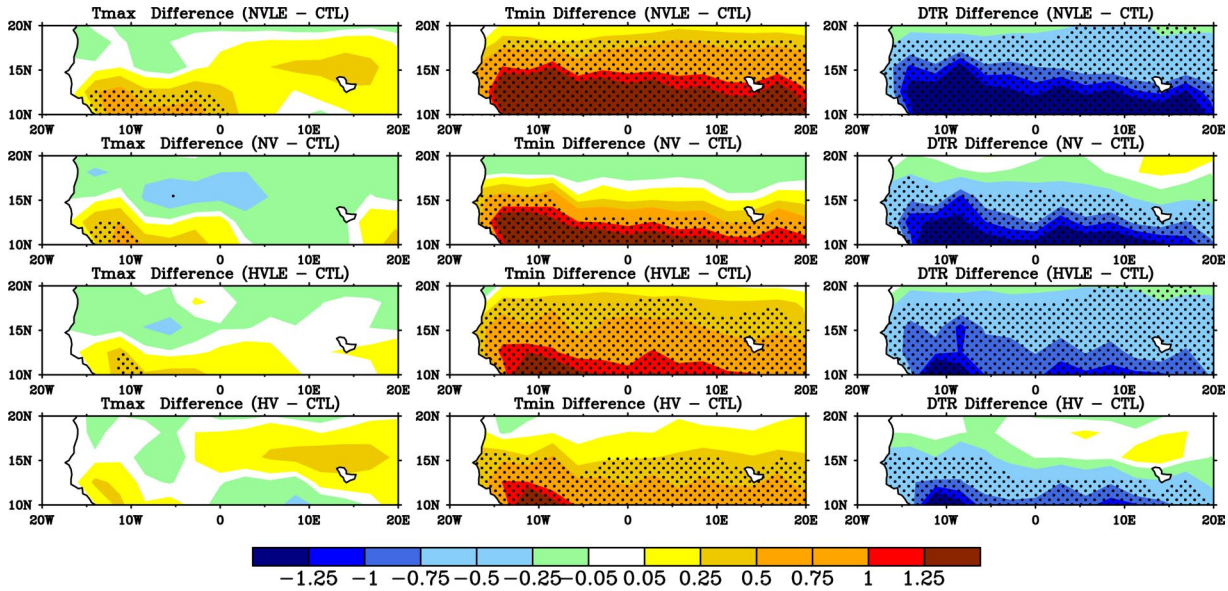

Fig. 3. Spatial patterns of simulated annual mean temperature differences (°C) between the four experiments (NVLE, NV, HVLE, and HV) and the control run (CTL) under clear-sky conditions in the Sahel. Daily averaged low cloud fraction <20% is defined as clear-sky conditions. Stippling shows grid cells where the temperature differences are statistically significant at the 5% level. A two-tailed Student's *t* test was used to test whether the difference differs significantly from zero.

conditions, defined as the daily averaged low cloud cover less than 20%, to filter out any effects of changes in clouds and rainfall on simulated DTR. Our results below show that such effects, however, are small. Another advantage of conditioning the analysis by clear-sky conditions is to reduce impacts of uncertainties in modeled clouds and their longwave radiation on DTR, especially in the wet season.

For a vegetated patch in a model grid cell, the fraction of ground longwave radiation that is shaded locally by vegetation is modeled by $1 - e^{-\mathrm{LSAI}}$, where LSAI represents leaf and stem area index. Hence, reduced vegetation cover exposes more soil directly to the atmosphere, increasing the importance of its lower emissivity on both the absorption and emission of longwave radiation. The observational 5° by 5° temperature data are available from 10°N to 20°N, 15°W to 20°E over the Sahel, largely overlapping the model grid cells with edges at 8.4°N to 19.5°N, 18.3°W to 21.1°E (SI Fig. 7). SI Fig. 8 shows the seasonal cycle of LSAI over the Sahel. The vegetation amount is very sparse beyond 16.7°N and increases southward between 8.4°N and 16.7°N. Over the latitude zone between 10°N and 17°N, there is 43.1% bare soil, 24.5% broadleaf deciduous shrub, 15.5% C_3 grass, 15.3% C_4 grass, and 1.7% broadleaf deciduous trees. Regional averaging of model outputs was performed over the center of model grid cells from 11.2°N to 16.7°N, 15.5°W to 19.7°E. Limiting the averaging to this region helps reduce impacts from surrounding land and ocean grid cells and allows the diurnal cycle of model variables to be composited with universal time.

Both the reduction of vegetation and the reduction of soil emissivity increase nighttime temperature much more than daytime temperature (Figs. 3–5). The simulated warming is strong and statistically significant for $T_{\min}$ over the majority of the model grid cells where the soil emissivity and/or vegetation cover were reduced, whereas the changes in $T_{\max}$ are insignificant (Fig. 3), i.e., any changes in $T_{\max}$ are of the same magnitude as random variability. Over most of the regions, the simulated DTR declines significantly. Among the four experiments, NVLE (HV) is the largest (smallest) in magnitude and spatial extent in its increase of $T_{\min}$ and thus its reduction of DTR. The simulated temperatures generally show the greatest increase at about 5–8 a.m. and the smallest increase at about 4–6 p.m. (Fig. 4). Note that the modeled $T_{\max}$ and $T_{\min}$ occur about 5 p.m. and 6 a.m., respectively, i.e., the effects of reduction in vegetation and soil emissivity are most effective in increasing $T_{\min}$. Regional averaged differences in the simulated annual mean $T_{\max}$ ($T_{\min}$) between CTL and NVLE, NV, HVLE, and HV are 0.21°C (1.22°C), −0.08°C (0.63°C), −0.01°C (0.72°C), and 0.1°C (0.46°C), and thus the DTR decreases by −1.01°C, −0.71°C, −0.73°C, and −0.36°C, respectively (Fig. 5).

To explain the effects of changes in vegetation and soil emissivity on surface air temperature, we sampled the diurnal cycle of related model variables at 3-hr intervals. The lowest

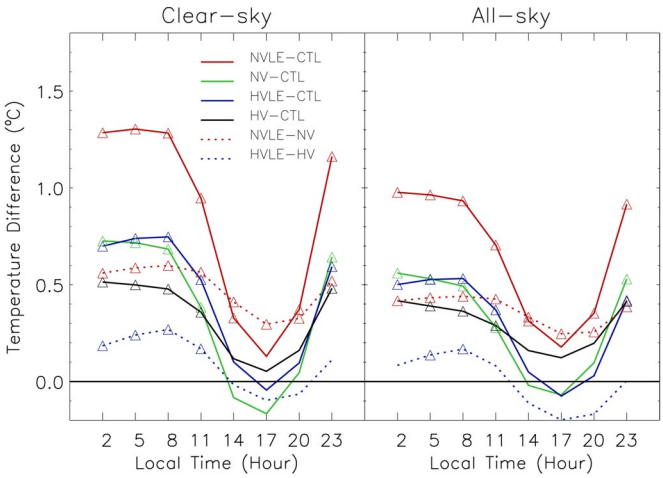

Fig. 4. Diurnal cycle of simulated annual mean $T_{\max}$, $T_{\min}$, and DTR differences (°C) among the four experiments (NVLE, NV, HVLE, and HV) and the control run (CTL) under clear-sky (*Left*) and all-sky (*Right*) conditions averaged over the Sahel. The model outputs are 3-hr averages from each time step (20 min). The clear-sky conditions are defined as in Fig. 3. In the simulations, the $T_{\max}$ occurs at about 5 p.m. and the $T_{\min}$ at about 6 a.m. The differences marked with △ are statistically significant at the 5% level. The significance test was done as for Fig. 3.

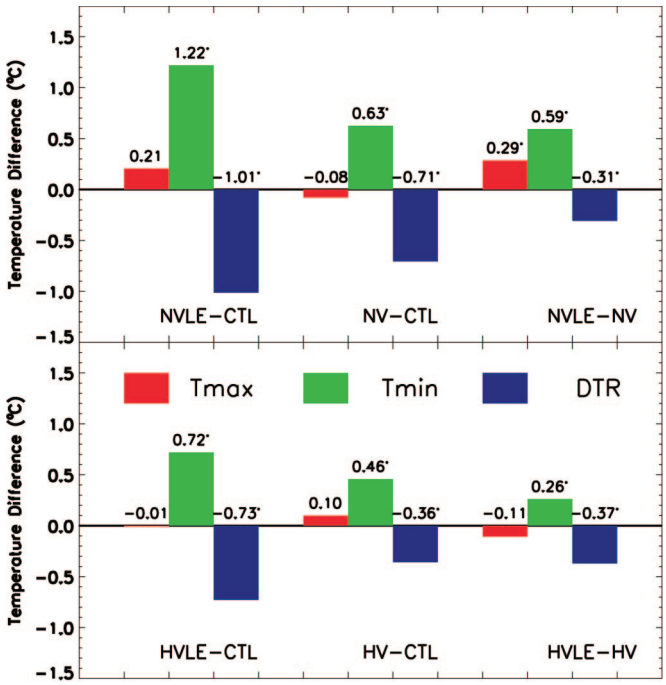

Fig. 5. Simulated annual mean T_{max}, T_{min}, and DTR differences (°C) among the four experiments (NVLE, NV, HVLE, and HV) and the control run (CTL) under clear-sky conditions averaged over the Sahel. The clear-sky conditions are defined as in Fig. 3. The temperature differences marked with * are statistically significant at the 5% level. The significance test was done as for Fig. 3.

atmospheric level temperature shows a similar but smaller increase as surface air temperature in the diurnal cycle, whereas the ground temperature increases more in daytime than in nighttime, consistent with the increased daytime ground absorption of solar radiation because of the removal of vegetation (SI Figs. 9–11). Changes in the diurnal cycle of annual mean radiation and energy budget averaged over the Sahel are shown in SI Fig. 12. Spatial patterns of differences in annual mean ground temperature, lowest atmospheric level temperature, net longwave radiation, outgoing longwave radiation, latent heat, sensible heat, soil fluxes, and net solar radiation are shown in SI Figs. 10, 11, and 13–18. Because these variables vary diurnally, our results are shown at daytime (4–6 p.m.) and nighttime (4–6 a.m.) when T_{max} and T_{min} occur. Changes in surface albedo, emissivity, and roughness, and validation of rainfall, latent heat, sensible heat, and Bowen ratio are shown in SI Figs. 19–21 and SI Table 2, and discussed in the *SI Text*. As expected, the removal of vegetation decreases the latent heat significantly during daytime but has little effect during nighttime (SI Fig. 15). It significantly increases the soil heat stored during daytime and released during nighttime (SI Fig. 17), and also decreases the daytime net solar radiation because of increased albedo (SI Fig. 18). The reduced soil emissivity reduces the outgoing longwave radiation, whereas the removal of vegetation has the opposite effect because vegetation with zero heat capacity reaches colder temperatures than the soil at night (SI Figs. 13 and 14). Consequently, the effect of lower soil emissivity on reducing the outgoing longwave radiation is most pronounced over nonvegetated regions (NVLE versus NV) but it is largely cancelled over vegetated regions (HVLE versus HV) (SI Figs. 12–14). During nighttime, increased soil heating (mainly over vegetated regions) and reduced outgoing longwave radiation (mainly over nonvegetated regions) are the two dominant factors in increasing the ground temperature and hence the air temperature and sensible heat for all experiments (SI Table 2). During daytime, decreased net solar radiation, reduced roughness, and increased soil heat storage (all mainly over vegetated regions), together with reduced outgoing longwave radiation (mainly over nonvegetated regions), decrease both the sensible and latent heat but with little changes of the air temperature. The daytime temperatures of the atmosphere are affected much less by a given change in radiation and energy budget because of the depth of the daytime convective boundary layer. When only the vegetation is removed, the increase of T_{min} is controlled by an increase of outgoing longwave radiation balancing the increased release of soil thermal storage. When the reduction of soil emissivity is also considered, the reduced outgoing longwave radiation further increases T_{min}.

The simulated warming is larger under clear-sky conditions than under all-sky conditions (Fig. 4 and SI Fig. 9) and is stronger in the dry season than in the wet season (data not shown). The modeled temperatures differ little in winter but vary significantly in summer between clear-sky and all-sky conditions, suggesting that the warming due to the reduction of soil emissivity and vegetation cover can be largely masked by the effects of increased clouds and vegetation in the wet season. The larger cloud amounts in summer sharply reduce solar heating during daytime and the larger vegetation coverage cools the surface through enhanced evapotranspiration. Consequently, less energy is stored during the daytime to increase nighttime temperatures.

Discussion and Conclusions

These results suggest a hypothesis that the reduction of vegetation cover and soil wetness may reduce the DTR by increasing nighttime surface air temperature during periods of drought and human mismanagement over semiarid regions such as the Sahel. If this hypothesis is true, one would expect to see a reversal of the DTR reduction with more rainfall and better human management. Recent analyses of satellite-measured greenness by using the NDVI indicate a greening trend of vegetation over the Sahel as a result of the increasing rainfall (38, 39), atmospheric CO_2 (40), and improved land management (41). The analysis of Fig. 2 shows a greening trend in the Sahel since 1984, and the negative trend of the Sahelian DTR appears to have stopped in 1991 and may have reversed after the recovery of rainfall starting in 1983. There is a statistically significant negative correlation between T_{min} and NDVI, whereas the relationship between T_{max} and NDVI is very weak (Table 1), as shown in previous studies (5, 42). Possibly, the increase of vegetation cover and soil moisture associated with the increase of rainfall reduces the T_{min} and thus increases the DTR, consistent with our simulations.

The amplitude of the diurnal cycle of temperatures over land can be changed through changes of energy and hydrological balances controlled by atmospheric composition, cloud properties, soil moisture, and vegetation. Changes in the land surface from climatic and anthropogenic forcing factors due to drought and human mismanagement (e.g., deforestation, land degradation, and soil erosion) could increase surface air temperature at night and decrease DTR through increased soil heating and reduced outgoing longwave radiation over semiarid regions such as the Sahel, a conclusion consistent with both empirical analyses and climate model simulations. Other mechanisms with similar effects on surface energy balance, such as increased nighttime downward longwave radiation because of increased greenhouse gases, aerosols, and clouds, would also be expected to have similar consequences for the DTR, and thus may account for the global correlation for a larger DTR reduction over drier regions (Fig. 1).

Our validation with limited site measurements indicates that the model adequately simulates the climatology of rainfall and surface fluxes over our study region (for details see the *SI Text* and SI Figs. 19–21). One deficiency in our simulations is the model's inability to simulate drought (see details in the *SI Text*).

The vegetation was not a dynamic component of the model, and interannual variations of sea surface temperature were not considered. No substantial rainfall reduction was simulated and thus no significant drought occurred in any of four experiments relative to the control run (SI Fig. 19). The aforementioned simulations showed a strong and significant warming in T_{min} and a small and insignificant warming in T_{max} (and thus the DTR decreased substantially) from the reduction of soil emissivity and vegetation. The magnitude of such changes was largest during dry seasons (largest Bowen ratio) and smallest during wet seasons (smallest Bowen ratio). If the model handled drought well, we would see a stronger warming in T_{min} and a larger decrease in DTR as a result of overestimated evapotranspiration (thus underestimated Bowen ratio) because more energy was dissipated into the form of latent heat rather than sensible heat that otherwise would be used to raise the temperature. Although there is no drought simulated in our experiments, the vegetation amount and soil emissivity were reduced to reflect drought-related changes as stated previously. Therefore, the inability to simulate drought in the model should not invalidate or weaken, but strengthen our conclusions resulting from the changes in vegetation and soil emissivity. Considering other uncertainties and limitations in the models and the observations (see the *SI Text*), we interpret our results as illustrative rather than definitive. However, this study draws attention to an important issue that requires further investigation. It is a step in the development of a quantitative basis for assessing the DTR change associated with drought and vegetation removal.

Data and Methods

We used a global dataset of monthly mean T_{max}, T_{min}, and DTR in each 5° by 5° latitude–longitude grid box processed from up to 7,018 meteorological stations across the world for the period of 1950–2004 (3). It covers 71% of the total land area, 17% more than in previous studies (2). We georeferenced the global monthly dataset of 2.5° by 2.5° precipitation (15) and 1° × 1° total cloud cover (16) for the period of 1950–2004, and the global bimonthly 8-km by 8-km NDVI dataset for the period of 1982–2004 (17) into the 5° by 5° latitude–longitude grid boxes of the temperature data (3). For each variable, the grid-box monthly time series anomalies were first generated by removing the climatological seasonal cycle within each box, and then temporally averaged to generate annual and seasonal mean time series anomalies. For the temperature data, only 552 grid boxes with at least 1 month of data for each season, at least 7 months of data for each year, and at least 31 years of data during the period of 1950–2004 were analyzed. Linear time trends were estimated by using ordinary least squares. A two-tailed Student's *t* test was used to test whether the trends differ significantly from zero. Area-weighed averaging was used to generate regional average values from the 5° by 5° grid boxes. Because there are some missing data during part of the period over some grid boxes, if one variable was missing, the other variables were also set as missing values for the time series analysis shown in Fig. 2 and Table 1.

We are grateful to two reviewers for their constructive suggestions on this article and to Garik Gutman and Chris Justice for their comments on the earlier version of this article. We thank Aiguo Dai for providing the cloud and Palmer Drought Severity Index data, A. Verhoef and H. A. R. de Bruin for providing the surface flux measurements of HAPEX-Sahel, and Dennis Baldocchi for providing the AmeriFlux site measurements of Vaira Ranch. The model simulations were supported by the National Center for Atmospheric Research computational facility. This study was supported by National Aeronautics and Space Administration Grants NNG04GK87G and NNG04GO61G.

1. Intergovernmental Panel on Climate Change (2001) *Climate Change 2001: The Scientific Basis* (Cambridge Univ Press, Cambridge, UK).
2. Easterling DR, Horton B, Jones PD, Peterson TC, Karl TR, Parker DE, Salinger MJ, Razuvayev V, Plummer N, Jamason P, *et al.* (1997) *Science* 277:364–367.
3. Vose RS, Easterling DR, Gleason B (2005) *Geophys Res Lett* 32:10.1029/2005GL024379.
4. Pinker RT, Zhang B, Dutton EG (2005) *Science* 308:850–854.
5. Zhou L, Dickinson RE, Tian Y, Fang J, Li Q, Kaufmann RK, Tucker CJ, Myneni RB (2004) *Proc Natl Acad Sci USA* 101:9540–9544.
6. Karl TR, Jones PD, Knight RW, Kukla G, Plummer N, Razuvayev V, Gallo KP, Lindseay J, Charlson RJ, Peterson TC (1993) *Bull Am Meteorol Soc* 74:1007–1023.
7. Dai A, Trenberth KE, Karl TR (1999) *J Clim* 12:2451–2473.
8. Collatz GJ, Bounoua L, Los SO, Randall DA, Fung IY, Sellers PJ (2000) *Geophys Res Lett* 27:3381–3384.
9. Hansen J, Sato M, Ruedy R (1995) *Atmos Res* 37:175–209.
10. Stone DA, Weaver AJ (2003) *Clim Dyn* 20:435–445.
11. Stenchikov GL, Robock A (1995) *J Geophys Res Atmos* 100:26211–26227.
12. Mitchell JFB, Davis RA, Ingram WJ, Senior CA (1995) *J Clim* 8:2364–2386.
13. Reader MC, Boer GJ (1998) *Clim Dyn* 14:593–607.
14. Huang Y, Dickinson RE, Chameides WL (2006) *Proc Natl Acad Sci USA* 103:4371–4376.
15. Chen M, Xie P, Janowiak JE, Arkin PA (2002) *J Hydrometeorol* 3:249–266.
16. Qian TT, Dai AG, Trenberth KE, Oleson KW (2006) *J Hydrometeorol* 7:953–975.
17. Tucker CJ, Pinzon JE, Brown ME, Slayback D, Pak EW, Mahoney R, Vermote E, El Saleous N (2005) *Int J Rem Sens* 26:4485–4498.
18. Zeng N, Neelin JD, Lau KM, Tucker CJ (1999) *Science* 286:1537–1540.
19. Hulme M (2001) *Glob Environ Change* 11:19–29.
20. Held IM, Delworth TL, Lu J, Findell KL, Knutson TR (2006) *Proc Natl Acad Sci USA* 103:1152–1153.
21. Intergovernmental Panel on Climate Change (2001) *Climate Change 2001: Impacts, Adaptation and Vulnerability* (Cambridge Univ Press, Cambridge, UK).
22. Salisbury JW, Daria DM (1992) *Rem Sens Environ* 42:83–106.
23. Urai M, Matsunaga T. Ishii T (1997) *Rem Sens Soc Jpn* 17:322–331.
24. Idso SB, Jackson RD, Reginato RJ, Kimball BA, Nakayama FS (1975) *J Appl Meteorol* 14:109–113.
25. Eltahir EAB (1996) *J Geophys Res Atmos* 101:4255–4268.
26. Claussen M (1997) *Clim Dyn* 13:247–257.
27. Zheng XY, Eltahir EAB (1998) *J Clim* 11:2078–2096.
28. Knorr W, Schnitzler KG, Govaerts Y (2001) *Geophys Res Lett* 28:3489–3492.
29. Zhou L, Dickinson RE, Tian Y, Jin M, Ogawa K, Yu H, Schmugge T (2003) *J Geophys Res Atmos* 108:10.1029/2003JD004083.
30. Dickinson RE, Oleson KW, Bonan G, Hoffman F, Thornton P, Vertenstein M, Yang ZL, Zeng XB (2006) *J Clim* 19:2302–2324.
31. Oleson K, Dai Y, Bonan G, Bosilovich M, Dickinson R, Dirmeyer P, Hoffman F, Houser P, Levis S, Niu G-Y, *et al.* (2004) *Technical Description of the Community Land Model (CLM)* (Natl Cent Atmos Res, Boulder CO), NCAR Techn Note, NCAR/TN-461+STR.
32. Tian Y, Dickinson RE, Zhou L, Shaikh M (2004) *J Geophys Res Atmos* 109:10.1029/2003JD004499.
33. Dickinson RE, Hendersonsellers A (1988) *Q J R Meteorol Soc* 114:439–462.
34. Charney JG (1975) *Q J R Meteorol Soc* 101:193–202.
35. Xue Y, Shukla J (1993) *J Clim* 6:2232–2245.
36. Ogawa K, Schmugge T (2004) *Earth Interact* 8:1–14.
37. Jin M, Liang S (2006) *J Clim* 19:2867–2881.
38. Hutchinson CF, Herrmann SM, Maukonen T, Weber J (2005) *J Arid Environ* 63:535–537.
39. Anyamba A, Tucker CJ (2005) *J Arid Environ* 63:596–614.
40. Hickler T, Eklundh L, Seaquist JW, Smith B, Ardo J, Olsson L, Sykes MT, Sjostrom M (2005) *Geophys Res Lett* 32:10.1029/2005GL024370.
41. Olsson L, Eklundh L, Ardo J (2005) *J Arid Environ* 63:556–566.
42. Gallo KP, Owen TW (1999) *J Appl Meteorol* 38:806–813.
43. Granger CWJ, Newbold P (1974) *J Econometrics* 2:111–120.